Korean J. Chem. Eng., 36(4), 613-619 (2019)
DOI: 10.1007/s11814-019-0242-x

pISSN: 0256-1115
eISSN: 1975-7220

Photoluminescence and photocatalytic properties of Eu^{3+}-doped $CaZnTiO_3$ perovskites with metal ion loading

Byung-Geon Park†

Department of Food and Nutrition, Kwangju Women's University, 165 Sanjung-dong, Gwangju 62396, Korea
(*Received 30 November 2018 • accepted 11 February 2019*)

Abstract−Europium (Eu^{3+})-doped $CaZnTiO_3$ perovskite phosphors were synthesized using a sol-gel reaction method. Different solvent materials were introduced to the synthesis process to produce higher emitting phosphors. Eu^{3+}-doped $CaZnTiO_3$ perovskite synthesized using an ethanol mixture solvent exhibited higher photoluminescence intensities for red emission than those synthesized using distilled water as a solvent. The synthesized Eu^{3+}-doped $CaZnTiO_3$ perovskites were characterized by photo-physical analysis and tested for the photocatalytic degradation of toluene. Ru, Co, and Ni ions were loaded on the perovskites to improve photocatalytic activity. Ni ion-loaded $CaZnTiO_3 : Eu^{3+}$ perovskite showed enhanced red emission and higher photocatalytic activities compared to those of bare $CaZnTiO_3 : Eu^{3+}$ perovskite. The improvement of the photocatalytic degradation of toluene was attributed to the lower bandgap of Ni ion-loaded $CaZnTiO_3 : Eu^{3+}$ perovskite, as determined by UV-visible diffuse reflectance spectroscopy.

Keywords: $CaZnTiO_3$, Perovskite, Europium, Photoluminescence, Photocatalytic Degradation

INTRODUCTION

Perovskites, which are used in numerous technological applications, exhibit a range of desirable properties [1-3]. They are compounds with the general formula, ABO_3. In general, larger cations are located in the A site, whereas smaller cations are located in the B site. The photoluminescence (PL) of the perovskites doped with rare-earth ions was studied with a consideration of the semiconducting properties, phase transitions, and ferroelectricity. In particular, considerable studies have been carried out to fabricate oxide phosphors, such as perovskites doped with rare-earth ions. Those have advantages over sulfide-based phosphors, such as chemical stability against electron bombardment and high vacuum [4].

Recently, many studies have reported the photoluminescence of highly emissive red-emitting titanates [5-10]. Rare earth ion-doped titanates have attracted considerable attention owing to the promising photoluminescence and potential applications to white light-emitting diodes (LEDs) [11]. Rare earth metal ion-doped calcium titanate ($CaTiO_3$) has excellent chemical tolerance, which can be applicable to LEDs [12,13].

White LEDs prepared from near UV excitation materials and corresponding perovskite phosphors have higher color stability [14]. A few studies have reported phosphors with near UV excitation [15,16]. Many studies on Eu-doped perovskites have been carried out because their luminescent center provides strong red emission. On the other hand, their applications are restrained because of the low luminous intensity in these perovskite-type hosts [17,18] or strong absorption of UV light [19,20]. LEDs with near-UV (~400 nm) excitation are well known and the development of new phosphors with near UV excitation is becoming an important issue.

Perovskite-based photocatalysts have been a concern in various fields of photocatalytic reactions [21,22]. Some perovskite materials have been developed for use as photocatalysts using visible light. $CaTiO_3$ has attracted interest because of its easy-preparation, excellent stability, and low-cost [23,24]. Photocatalytic properties for various photocatalysts are tested in a typical photocatalytic decomposition of organic materials [25-27].

In this study, Eu^{3+}-doped $CaZnTiO_3$ perovskite phosphors were synthesized using a sol-gel reaction method. Different solvent materials were introduced to obtain higher emitting phosphors in the synthesis process. The structures and basic properties of $CaZnTiO_3 : Eu^{3+}$ and metal-loaded $CaZnTiO_3 : Eu^{3+}$ perovskites were characterized, and their photo-physical properties were examined using the excitation and emission spectra. The photocatalytic ability of the $CaZnTiO_3 : Eu^{3+}$ perovskites for the degradation of toluene was evaluated. Ru, Co, and Ni ions were loaded on the perovskites to improve photocatalytic activity.

EXPERIMENTAL SECTION

1. Preparation of Materials

Eu-doped $CaZnTiO_3$ was prepared using the sol-gel method based on the $CaZnTiO_3 : Eu^{3+}$ formula with different basic solvent materials. Distilled water or an ethanol mixture was used as the basic solvent for the synthesis $CaZnTiO_3 : Eu^{3+}$ phosphors. Stoichiometric amounts of $Zn(NO_3)_2 \cdot 6H_2O$, $Ca(NO_3)_3 \cdot 4H_2O$, and $Eu(NO_3)_3 \cdot 6H_2O$ were introduced as the starting materials. $Ca(NO_3)_3 \cdot 4H_2O$ (94.45 g), $Zn(NO_3)_2 \cdot 6H_2O$ (29.75 g), and $Eu(NO_3)_3 \cdot 6H_2O$ (8.90 g) were added to distilled water with vigorous stirring at 80 °C for 3 h. Subsequently, $Ti(OC_4H_9)_4$ (170.15 g) was inserted in the solution with stirring for 2 h. The solution was dried at 110 °C for one day. The resulting solid was evacuated and heated to 1,100 °C in a

†To whom correspondence should be addressed.
E-mail: bgpark814@naver.com

furnace at 5 °C/min and held at that temperature for 5 h. The calcined-materials were crushed to obtain a fine powder.

An ethanol (100 mL), 2-methoxyethanol (50 mL), and citric acid (10 g) mixture was prepared as the basic solvent in the sol-gel process. $Ca(NO_3)_3{\cdot}4H_2O$, $Zn(NO_3)_2{\cdot}6H_2O$, and $Eu(NO_3)_3{\cdot}6H_2O$ were added to the basic solvent with vigorous stirring at 80 °C for 3 h. $Ti(OC_4H_9)_4$ was then introduced in the solution with stirring for 2 h. The solution was dried at 110 °C for one day. The resulting solid was evacuated and heated to 1,100 °C in a furnace at 5 °C/min and held at that temperature for 5 h. The calcined-materials were crushed to obtain a fine powder. The Eu-doped $CaZnTiO_3$ perovskites obtained from the distilled water solvent and ethanol mixture solvent are called CTO and CTO-E, respectively.

Metal-doped CTO-E perovskites were prepared using a typical incipient impregnation method. Ruthenium(III) chloride hydrate ($RuCl_3{\cdot}xH_2O$, Aldrich, 99.98%), cobalt(II) chloride hexahydrate ($CoCl_2{\cdot}6H_2O$; Junsei, 99.9%), and nickel(II) nitrate hexahydrate ($Ni(NO_3)_2{\cdot}6H_2O$; Junsei, 99.9%) were used as the Ru, Co, and Ni metal resources. The metal loading in the CTO-E phosphors was adjusted to 2 wt%. Metal-doped CTO-E perovskites were also dried at 110 °C and calcined at 1,100 °C. The calcined perovskites were crushed to a fine powder.

2. Characterization of the Perovskites and Photoluminescence Spectroscopy

The crystallinity and structures of the perovskite photocatalysts were examined by high resolution X-ray diffraction (XRD, Rigaku model Dmax-II/PS) using Ni filtered CuKα X-ray radiation (λ= 1.5405 Å). The morphology and microstructure of the perovskites were measured by field emission scanning electron microscope (FE-SEM, Hitachi, S-4810). The fluorescence spectrum was recorded using a fluorescence spectrophotometer (Horiba, Fluoromax-4). The N_2 isotherms of the photocatalysts were estimated using the volumetric adsorption apparatus (MSI, Nanoporosity-XQ) at liquid nitrogen temperature. The photocatalysts were pretreated at 200 °C for 2 h before exposure to N_2 gas. Their surface areas were calculated by the BET equation.

The chemical components of the perovskites were measured using energy dispersive X-ray spectroscopy (EDX, NORANE Z-MAXI 350). UV-visible diffuse reflectance spectroscopy (DRS, Shimadzu, UV-2500) was performed over the 200-1,000 nm wavelength range using $BaSO_4$ as a reflectance standard. The optical bandgap (E_{gap}) was determined from Kubelka-Münk theory. Fourier transform infrared (FT-IR) spectroscopy was measured on a JASCOS FT-IR-500 plus spectrometer. The samples were diluted (10%) in KBr and scanned over the frequency range of 400-4,000 cm^{-1} at room temperature.

The PL spectra were estimated using a PL spectrometer (Spectrograph 500i, Actons Research Co., USA), and an intensified CCD (PI-MAX3) (IRY1024, Princeton Instrument Co., USA) with 150 grooves/mm grating (blazing wavelength: 300 nm). The excitation light source was a 266 nm DPSS laser, and the laser power applied to the sample surface was 12.5 mW. The exposure time was 100 msec at room temperature.

3. Photocatalytic Degradation of Toluene

The photocatalysts were added to a toluene solution (80 mL). The photocatalyst dose was controlled to 5 mL due to the significant difference in the densities between TiO_2 and the perovskites. The reactant and photocatalysts mixture was stirred in the dark for 1 h to reach adsorption equilibrium. The mixture was illuminated by UV-A light with stirring. Samples were taken at regular intervals to analyze the toluene concentration. The concentration of toluene in the samples was analyzed by gas chromatography (Hewlett Packard, HP5890). The photocatalytic degradation of toluene was in a glass reactor with a UV lamp system installed. The reactor was kept in the dark to prevent the dispersion of UV light during the photochemical reaction. The temperature of the photochemical reaction was kept at 25 °C. The UV lamp array consisted of two 15 W UV-A lamps. The light strength and UV irradiation was 30 Lx and 365 nm, respectively.

RESULTS AND DISCUSSION

1. Characteristics of the CTO Perovskites

Fig. 1 presents XRD patterns of the CTO perovskites. A comparison of the XRD pattern with the reference revealed good correspondence of the intensities and positions of the primary peaks with the data of the JCPDS card (No. 22-0153), as shown in Fig. 1. The XRD patterns were indexed to orthorhombic $CaTiO_3$. Zn_2TiO_4, and $Ca_2ZnTi_{15}O_{36}$ peaks, but their intensity was quite weak. The intensity of the primary phases of $CaTiO_3$ was not affected. The XRD patterns of CTO and CTO-E were similar. The XRD patterns with different calcinations temperature were almost the same with those over 800 °C of calcination temperature. This indicates that the crystallinity of the perovskites calcined over 800 °C was almost the same. This suggests that the perovskite was crystallized through calcination over 800 °C.

Fig. 2 shows FE-SEM images of the surface morphology of the CTO and CTO-E perovskites. Particles of the two perovskites were submicron-sized crystallites, which were agglomerates of smaller crystallites due to the high sintering temperatures. The shape of the perovskites was an agglomerated irregular cubic structure. The small crystallites were incorporated onto the aggregated crystallites. The

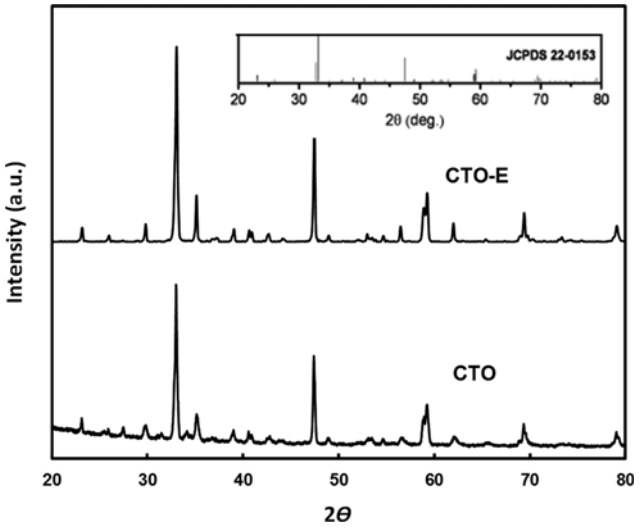

Fig. 1. XRD patterns of CTO and CTO-E perovskites with reference XRD pattern of JCPDS card.

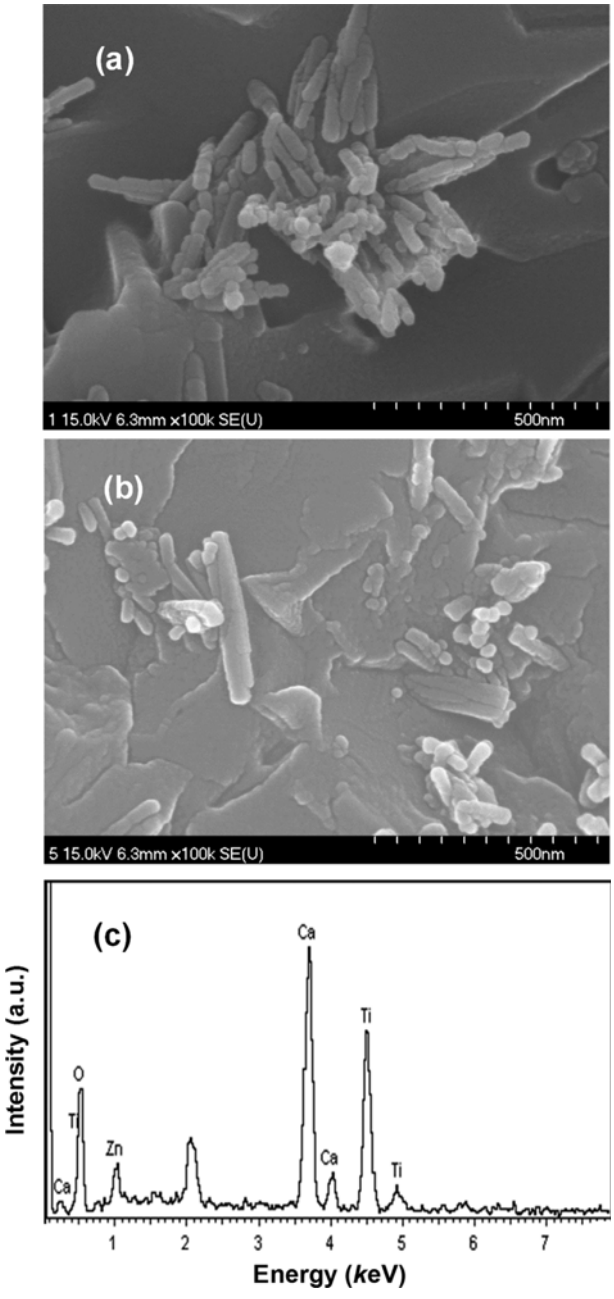

Fig. 2. FE-SEM images of (a) CTO and (b) CTO-E perovskites with (c) EDX spectrum of CTO perovskite.

grains were spherical polyhedrons, approximately 3 μm in size. Fig. 2(c) shows representative EDX spectra of the CTO perovskites. The EDX spectrum of the CTO exhibited the peaks related to Ca, Zn, and Ti. Eu was not observed because the content in the compound was too small. The effective radii of Ca^{2+}, Ti^{4+}, and Eu^{3+} ions in the octahedral site were 1.00, 0.605, and 0.947 Å, respectively [28]. This suggests that the Eu^{3+} ion can substitute easily for the Ca^{2+} ion in the $CaZnTiO_3:Eu^{3+}$ lattice compared to the Ti^{4+} ion because the ionic radii of Ca^{2+} and Eu^{3+} ions are closer. In addition, the orthorhombic lattices of $CaZnTiO_3:Eu^{3+}$, which represent the substitution of a Eu^{3+} ion for Ca^{2+} ion in the octahedral sites, were simulated [29].

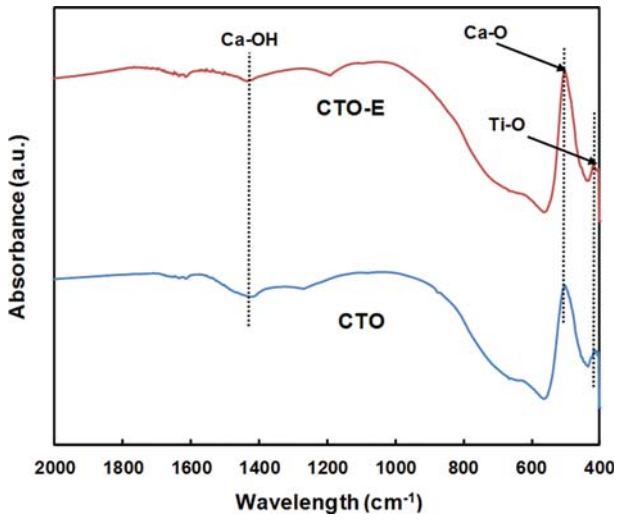

Fig. 3. FT-IR spectrum of CTO and CTO-E perovskites.

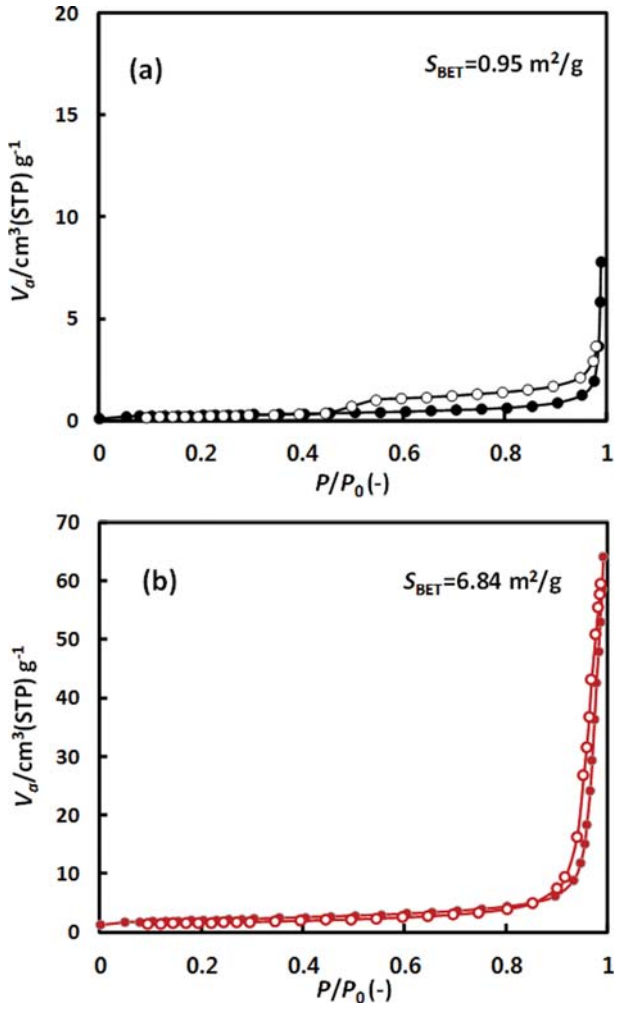

Fig. 4. N_2 isotherms of (a) CTO and (b) CTO-E perovskites.

Fig. 3 shows the FT-IR spectra of the CTO and CTO-E perovskites at 400-2,000 cm^{-1}. The spectra of two materials were almost similar. The broad peak at 3,423 cm^{-1} was assigned to the stretch-

ing vibrations of a hydroxyl group (-OH) due to water, and the bending band was observed at 1,650 cm^{-1}. The peak at 877 cm^{-1} was attributed to the symmetric stretching vibrations along the Ca-O-Ca bonds. The band at 1,439 cm^{-1} was assigned to the asymmetrical stretching vibration of the hydroxylate (OH-Ca). The band at 560 cm^{-1} was attributed to the vibration of the Ca-O bond of CTO and CTO-E. A broad and strong band, which is characteristic of alkaline titanates, was observed at 460 cm^{-1}. The band at 421 cm^{-1} was assigned to the asymmetrical stretching vibrations of Ti-O band.

Fig. 4(a) presents the N_2 isotherm of CTO perovskites. The amount of nitrogen adsorption was very small, and the BET specific area was less than 1 m^2/g. From these results, it is surmised that the CTO perovskites are nonporous crystalline materials. A hysteresis loop was observed in the adsorption-desorption curves. The hysteresis was driven from the void between the CTO particles because the CTO perovskite was nonporous. Fig. 4(b) presents the N_2 isotherm of CTO-E perovskite. The amount of nitrogen adsorption was increased compared to that of CTO perovskite. BET specific surface area was also significantly larger than that of CTO perovskite. It would appear that the CTO-E perovskite was also nonporous.

Fig. 5(a) presents UV-vis DRS of CTO perovskites and TiO_2 photocatalysts expressed as Kubelka-Münk units. The optical properties of the photocatalysts were initiated by light absorption in the photochemical processes. The spectrum of TiO_2 shows an adsorption edge at ca. 380 nm. In contrast, the adsorption edges of the CTO perovskites shifted to a longer wavelength of ca. 400 nm.

Fig. 5(b) presents UV-vis DRS of Ru, Co, and Ni ion-loaded CTO-E perovskites expressed as Kubelka-Münk units. The DRS of various metal-loaded CTO-E perovskites appeared in the upper light range compared to that of TiO_2. The adsorption range of Ru/CTO-E was lower than that of CTO-E due to the Ru ion loading. On the other hand, the adsorption range of Ni/CTO-E was larger than that of CTO-E perovskite. The adsorption edges of Ru/CTO-E, Co/CTO-E, and Ni/CTO-E were 395 nm, 400 nm, and 410 nm, respectively. The bandgaps of the metal ion-loaded CTO-E perovskites were similar, ranging from 3.0 eV to 3.2 eV. This suggests that the photosensitivity of Ni/CTO-E was improved by the Ni ion loading on the parent CTO-E perovskite.

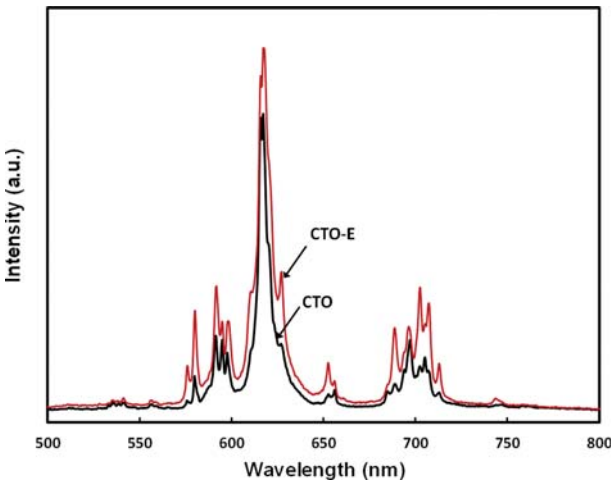

Fig. 6. PL spectra of CTO and CTO-E perovskites.

2. Photoluminescence Properties

Fig. 6 presents the PL emission spectra of CTO and CTO-E perovskites. The perovskites exhibited strong luminescence under UV excitation. CTO shows an emission intensity at 616 nm. A special emission of Eu^{3+} was not defined in the spectrum. The Eu^{3+} in the precursor was reduced to Eu^{2+} due to the weak reducing atmosphere. The Eu^{2+} in the precursor was reduced to Eu^{+}. Simultaneously, local vibrations in the lattice structure and thermal vibrations of the surrounding ions resulted in luminescence spectra with a broad band [30]. The PL intensity of the CTO-E phosphor was higher than that of the CTO phosphor under the same measuring conditions between the two materials. This suggests that the ethanol mixture solvent in the preparation process caused an enhancement of the emission properties. It appears that the solvent would lead to a better dispersion of Eu^{3+} ions than distilled water in the texture of the perovskite. This presents a similar tendency with the

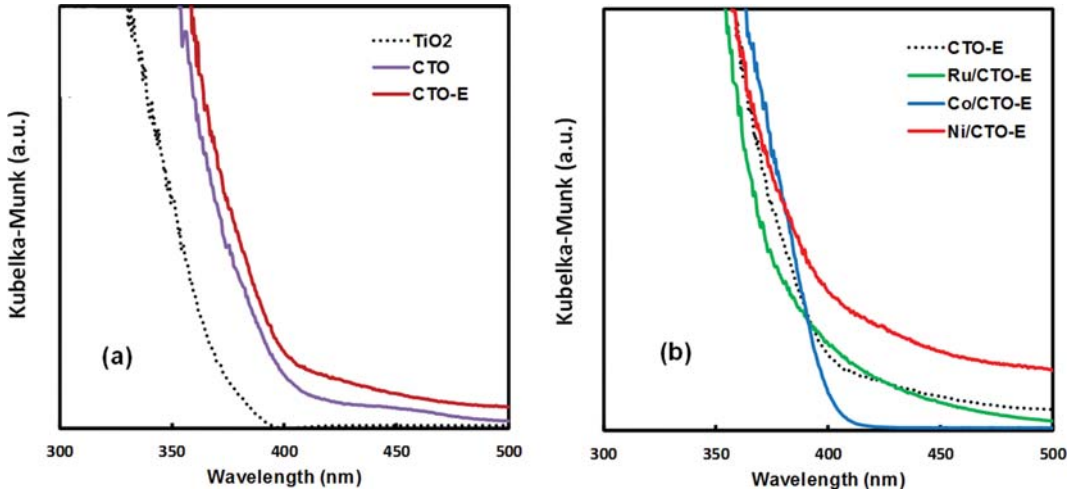

Fig. 5. DRS data of (a) CTO and (b) metal-loaded CTO-E.

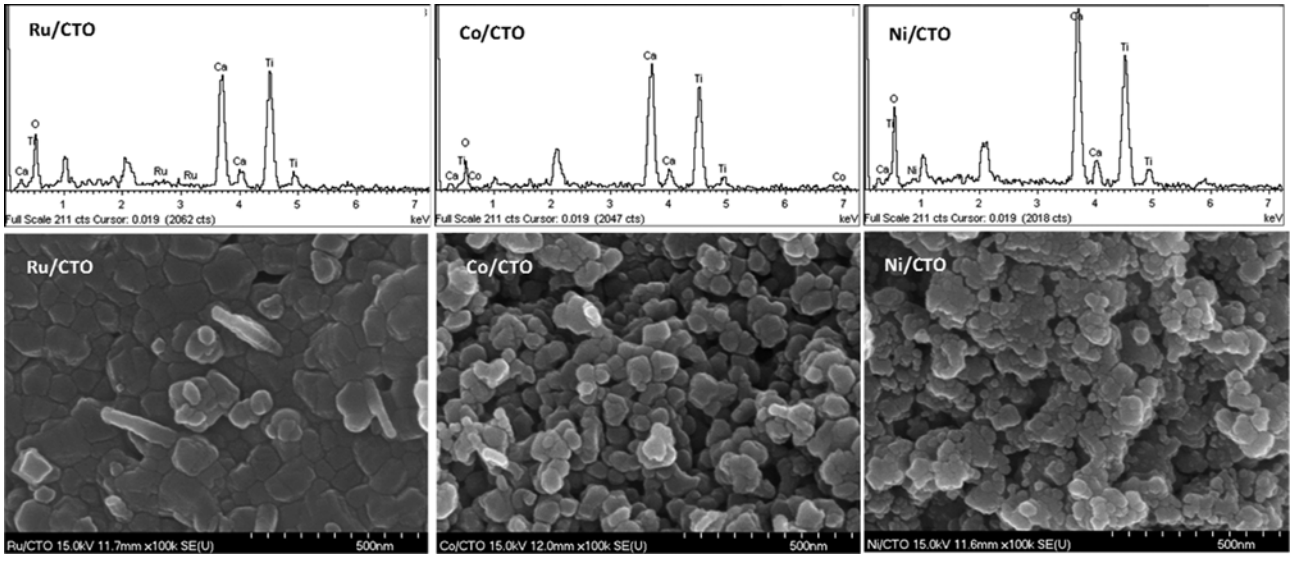

Fig. 7. EDX spectra and FE-SEM images of Ru, Co, and Ni-loaded CTO-E perovskites.

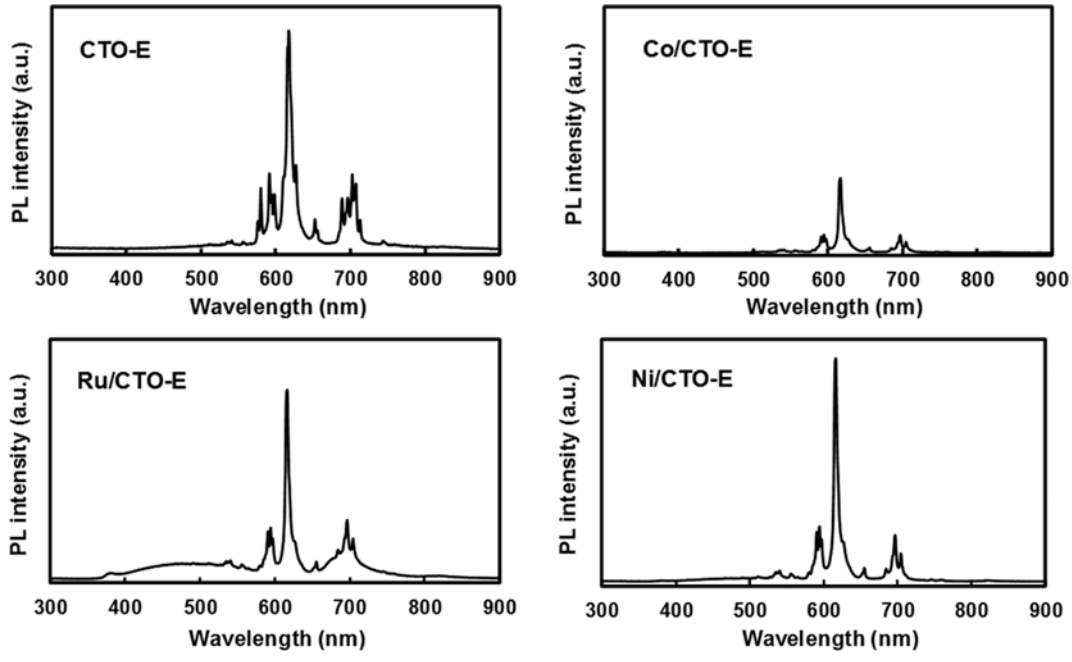

Fig. 8. PL spectra of CTO-E and metal ions-loaded CTO-E perovskites.

results of other literatures defined for $SrAl_2O_4:Eu^{2+},Dy^{3+}$ and $CaTiO_3:Eu^{3+}$ materials [31,32].

Fig. 7 presents EDX spectra and FE-SEM images of Ru, Co, and Ni metal loaded on Eu-doped CTO-E perovskite. The metal peaks were observed in the EDX spectra. The loading of Ru, Co, and Ni metals determined from the EDX results was 1.7 wt%, 1.8 wt%, and 1.8 wt%, respectively. The morphology of the Ru/CTO-E perovskite observed from the FE-SEM images was a flake shape. Those of Co/CTO-E and Ni/CTO-E were an irregular cubic shape. The particle sizes of the metal-loaded CTO-E perovskites were ca. 100 nm. The size of particles of the metal-loaded CTO-E was smaller and more uniform than those of bare CTO-E perovskite.

Fig. 8 presents the PL spectra of metal ion-loaded CTO-E perovskites. The PL intensity of Ru/CTO-E was reduced compared to that of the parent CTO-E perovskite, whereas the PL intensity of Co/CTO-E perovskite was similar to that of the parent CTO-E perovskite. This suggests that the Co ion loading on CTO-E was unaffected by the PL properties. In contrast, the PL intensity of Ni/CTO-E perovskite at 617 nm was higher than that of the parent CTO-E perovskite. In contrast, the other PL intensities at 595 nm and 700 nm were lower. Specifically, the red light emission was enhanced because the emission was concentrated at 617 nm.

3. Photocatalytic Properties of the CTO Perovskites

Fig. 9(a) shows the changes in the fraction of the remaining con-

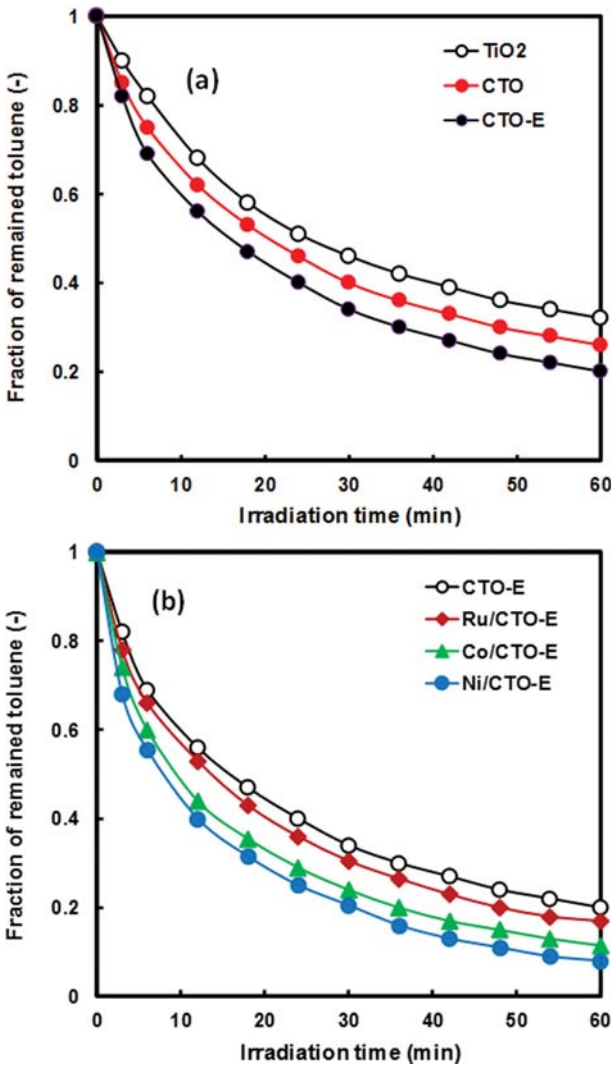

Fig. 9. Conversion of toluene by photocatalytic degradation on various CTO perovskite photocatalysts.

centration of toluene on the TiO_2 and CTO perovskite photocatalysts. The definition of the Y axis in Fig. 9 means 1-[(actual concentration of toluene)/(initial concentration of toluene)]. The toluene concentrations decreased because of the photocatalytic decomposition of toluene. The rate of toluene degradation was faster on the CTO perovskites than on the TiO_2 photocatalyst. A large amount of toluene might be adsorbed on the TiO_2 surface, which can prevent the toluene molecules from coming in contact with the free radicals and electron holes. The rate of toluene degradation was higher on CTO-E perovskite than CTO perovskite. This suggests that the lower bandgap of CTO-E resulted in the faster decomposition of toluene. The CTO-E showed a wider UV-visible absorption spectrum than CTO in the results of DRS analysis. Therefore, the higher photosensitivity would lead to enhanced photocatalytic activity in the photodegradation of toluene.

Fig. 9(b) shows the photocatalytic degradation of toluene on various metal-loaded CTO-E perovskites at 50 mg/L of the initial toluene concentration. The degradation of toluene on the Ni/CTO-E photocatalyst was faster than that on the other metal-loaded photocatalysts. This means that Ni/CTO-E has higher photocatalytic activity than the other metal ion-loaded CTO-E perovskites. The enhanced photocatalytic activity of Ni/CTO-E was attributed to its higher photosensitivity because Ni/CTO-E had a lower bandgap than the other metal ion-loaded CTO-E perovskites according to the DRS results. Therefore, a lower bandgap of Ni/CTO-E perovskite would lead to enhanced photocatalytic activity.

CONCLUSION

Eu^{3+}-doped $CaZnTiO_3$ perovskite phosphors were synthesized by a sol-gel reaction method with different solvent materials, such as distilled water and an ethanol mixture. $CaTiO_3:Eu^{3+}$ perovskite synthesized using the ethanol mixture solvent exhibited higher photoluminescence properties for red emission than that synthesized using distilled water. $Ni/CaZnTiO_3:Eu^{3+}$ perovskite exhibited enhanced red emission and higher photocatalytic activities for the degradation of toluene compared to that of bare $CaZnTiO_3:Eu^{3+}$ perovskite. The improvement of the photocatalytic degradation of toluene on $Ni/CaZnTiO_3:Eu^{3+}$ perovskite was attributed to the lower bandgap of the perovskite photocatalyst.

ACKNOWLEDGEMENTS

This paper was supported by Research Funds of Kwangju Women's University in 2018.

REFERENCES

1. P. Kanhere and Z. Chen, *Molecules*, **19**, 19995 (2014).
2. B. A. Josephine, A. Manikandan, V. M. Teresita and S. A. Antony, *Korean J. Chem. Eng.*, **33**, 1590 (2016).
3. K. Zhao, F. He, Z. Huang, G. Wei, A. Zheng, H. Li and Z. Zhao, *Korean J. Chem. Eng.*, **34**, 1651 (2017).
4. W. Chen, R. Sammynaiken and Y. Huang, *J. Appl. Phys.*, **88**, 1424 (2000).
5. S. Lazaro, J. Milanez, A. T. de Figueiredo, V. M. Longo, V. R. Mastelaro, F. S. DeVicente, A. C. Hernandes, J. A. Varela and E. Longo, *Appl. Phys. Lett.*, **90**, 111904 (2007).
6. Y. Pan, Q. Su, X. Xu, T. Chem, W. Ge, C. Yang and M. Wu, *J. Solid State Chem.*, **174**, 69 (2003).
7. D. Haranath, A. F. Khan and H. Chander, *J. Phys. D: Appl. Phys.*, **39**, 4956 (2006).
8. V. S. Marques, L. S. Cavalcante, J. C. Sczancoski, D. P. Volanti, J. W. M. Espinosa, M. R. Joya, M. R. M. C. Santos, P. S. Pizani, J. A. Varela and E. Longo, *Solid State Sci.*, **10**, 1056 (2008).
9. S. Okamoto and H. Kobayashi, *J. Appl. Phys.*, **86**, 5594 (1999).
10. X. Zhang, J. Zhang, M. Wang, X. Zhang, H. Zhao and X. J. Wang, *J. Lumin.*, **128**, 818 (2008).
11. X. M. Liu, P. Y. Jia and J. Liu, *J. Appl. Phys.*, **99**, 124902 (2006).
12. W. Jia, D. Jia, T. Rodriguez, D. R. Evans, R. S. Meltzer and W. M. Yen, *J. Lumin.*, **119**, 13 (2006).
13. X. M. Zhang, J. H. Zhang, Z. G. Nie, M. Y. Wang, X. G. Ren and X. J. Wang, *Appl. Phys. Lett.*, **90**, 151911 (2007).
14. J. Fu, Q. Zhang, Y. Li and H. Wang, *J. Lumin.*, **130**, 231 (2010).
15. J. S. Kim, P. E. Jeon, J. C. Choi, H. L. Park, S. I. Mho and C. G. Kim,

Appl. Phys. Lett., **84**, 2931 (2004).
16. P. J. Deren, R. Pazik, W. Strek, Ph. Boutinaud and R. Mahiou, *J. Alloys Compd.*, **451**, 595 (2008).
17. A. Bao, C. Tao and H. Yang, *J. Lumin.*, **126**, 859 (2007).
18. I. Omkaram, B. V. Rao and S. Buddhudu, *J. Alloys Compd.*, **474**, 565 (2009).
19. X. Gao, L. Lei, C. Lv, Y. Sun, H. Zheng and Y. Cui, *J. Solid State Chem.*, **181**, 1776 (2008).
20. H. Zhang, X. Fu, S. Niu and Q. Xin, *J. Alloys Compd.*, **459**, 103 (2008).
21. Q. Jia, A. Iwase and A. Kudo, *Chem. Sci.*, **5**, 1513 (2014).
22. K. Sayama, K. Mukasa, R. Abe, Y. Abe and H. Arakawa, *Chem. Commun.*, **23**, 2416 (2001).
23. H. Zhang, G. Chen, X. He and J. Xu, *J. Alloys Compd.*, **516**, 91 (2012).
24. Q. Fu, J. L. Li, T. He and F. W. Yang, *J. Appl. Phys.*, **113**, 104303 (2013).
25. Y. S. You, K.-H. Chung, J.-H. Kim and G. Seo, *Korean J. Chem. Eng.*, **18**, 924 (2001).
26. B.-G. Park, *Catalysts*, **8**, 227 (2018).
27. F.-F. Chen, K. Huang, J.-P. Fan and D.-J. Tao, *AIChE J.*, **64**, 632 (2018).
28. R. D. Shannon, *Acta Cryst.*, **A32**, 751 (1976).
29. T. M. Mazzo, M. L. Moreira, I. M. Pinatti, F. C. Picon, E. R. Leite, I. L. V. Rosa, J. A. Varela, L. A. Perazolli and E. Longo, *Opt. Mater.*, **32**, 990 (2010).
30. Q. Xiao, L. Xiao, Y. Liu, X. Chen and Y. Li, *J. Phys. Chem. Solids*, **71**, 1026 (2010).
31. H. Du, W. Shan, L. Wang, D. Xu, H. Yin, Y. Chen and D. Guo, *J. Lumin.*, **176**, 272 (2016).
32. J. Fu, Q. Zhang, Y. Li and H. Wang, *J. Alloys Compd.*, **485**, 418 (2009).